

The Application of Optically-based NDE Techniques to Flaw Detection in Aircraft Components

D.J. Reid Rowland, D. Findeis, J. Gryzagoridis

University of Cape Town, Private Bag, Rondebosch, 7700, South Africa
dave_reid_rowland@hotmail.com, dfindeis@eng.uct.ac.za, profg@eng.uct.ac.za

Abstract

This paper reports on the investigation into the use of two optical NDT techniques, namely Electronic Speckle Pattern Interferometry (ESPI) and Shearography to detect flaws in aircraft components. These techniques are both able to provide almost instantaneous results over a large inspection area. ESPI is a technique that compares the surface displacement profile of an object in its stressed and unstressed states. ESPI is used to locate flaws in a helicopter tail rotor section and a composite aircraft fin section with induced flaws. The fin section had not seen service, and manufacturing defects were also investigated. The technique proved successful in locating surface flaws in the tail rotor section and near-surface flaws in the fin section. Shearography is a technique that measures the change in displacement gradient or slope of an object's surface as a result of an applied stress. Shearography was used to detect delaminations between the spar and outer skin on Alouette III helicopter blades, and the results confirmed with Mechanical Impedance Analysis (MIA). Traditionally these blades are tested using finely tuned tapping hammers, which is a slow and tedious process. The shearography results generally compared favourably with the MIA results, indicating that this may be a viable technique for improving the NDT investigation of these blades.

Keywords

Non Destructive Testing, Electronic Speckle Pattern Interferometry, Mechanical Impedance Analysis, Shearography, Flaw detection, Aircraft components

Introduction

There is currently a wide array of techniques available in the field of Non-Destructive Testing. Some techniques are clearly better suited to particular situations and requirements and it is up to the investigator to choose a technique that will give the best results for that application. It is also possible to use more than one of these in conjunction with each other in order to make use of the benefits of each method. Three methods, Electronic Speckle Pattern Interferometry (ESPI), Shearography, Mechanical Impedance Analysis (MIA) and their application to flaw detection in aircraft components are described in this paper.

ESPI and Shearography are optical techniques that give rapid, qualitative information about a flaw. They are not, however able to give specific information such as size, shape or severity about the flaw. They can be used to locate flaws rapidly, which must be quantified by alternative techniques. MIA is a technique that gives precise information about the size and severity of a flaw based on the local stiffness and damping properties of the object, but is a time consuming process.

ESPI was used to detect flaws in a fibreglass/epoxy composite fin section and induced flaws in a helicopter tail rotor section. Although these were all visible surface flaws the technique is just as suited to subsurface flaws, as long as the defect affects surface displacement under applied loading. Shearography was used to highlight possible areas of delamination on worn helicopter blades from an Allouette III helicopter. MIA was then used to zoom in on the highlighted areas and quantify the flaws with regard to shape and size, and confirm or refute the shearography results.

Electronic Speckle Pattern Interferometry

ESPI is a NDT technique that relies on optical interference to measure the change in surface displacement of an object as a result of an applied stress. It had its origins on Holographic Interferometry and was first demonstrated in 1971[7] The technique measures relative surface displacement and is capable of measuring displacements in the order of half the wavelength of the light used (e.g. $0.3\mu\text{m}$ for Helium-Neon laser $\lambda=632\text{nm}$). [1] ESPI can be used for flaw

detection, design evaluation and vibration measurement. [3] A typical ESPI arrangement is shown in Figure 1.

A laser beam is split into a reference beam and object beam at the beam splitter. The object beam is used to illuminate the object. A psychedelic pattern of light and dark spots, known as speckle is formed on the object surface by interference of this illumination with itself. This speckle pattern is then reflected from the object surface and recorded by the camera CCD. The CCD is the part of the camera that is used to capture the image information. The reference beam is steered

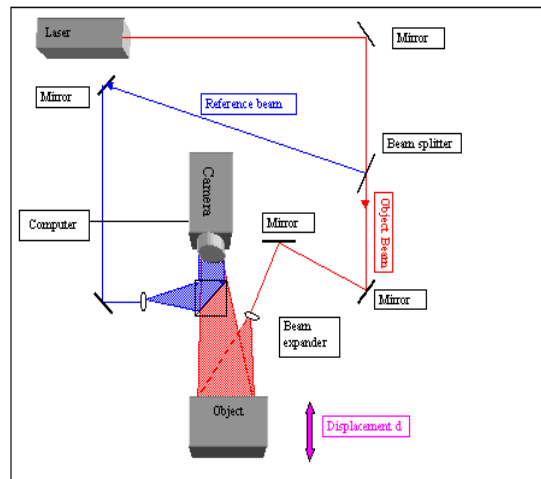


Figure 1 ESPI layout

directly onto the camera CCD via a prism and the object beam and reference beam combine and interfere with each other. This interference means that the speckle pattern is unique for the object's current position. If the object is displaced, the path length of the object beam changes, while the reference beam remains unchanged and a new speckle pattern is produced. The above layout is sensitive to out-of-plane displacement (displacement normal to the object surface), although several other variables such as in-plane displacement and their first and second derivatives can be measured by alternative layouts.

A typical ESPI inspection would be performed as follows: A speckle pattern of the object is captured in its unstressed state. The object is then stressed by application of one of a variety of methods, which include external mechanical forces, thermal, vacuum, and pressure. This causes the surface profile to change and hence the speckle pattern. The altered speckle pattern is then captured and the two speckle patterns are then digitally subtracted from each other by the computer, generating a zebra-like fringe pattern. The fringe pattern represents a 'contour map' of surface displacement, and each fringe line represents points on the object surface that have been displaced by equal amounts. Flawed regions will clearly deform more than other areas due to a reduction in strength, and are characterised by rapid changes in fringe density or direction in the fringe pattern.

The magnitude of the surface displacement at any point relative to another can be calculated by counting the number of fringes between the two points on the ESPI image and applying the following formula:

$$d_n = \frac{n\lambda}{\cos\theta_i + \cos\theta_c} \quad \text{Eqn 1}$$

Which for small camera and illumination angles can be simplified to

$$d_i = \frac{n\lambda}{2} \quad \text{Eqn 2}$$

Where n is the number of fringes observed

λ is the wavelength of light used

θ_i is the angle of illumination to the surface normal

θ_c is the angle of the camera axis to the surface normal of the object [2,7]

ESPI is extremely sensitive to environmental vibration, which must be eliminated if ESPI is to be successfully performed. Random motion of the object causes the object beam path length to change, and corrupts any results obtained. Typically ESPI is performed on a vibration-isolation table or with the use of pulsed lasers. [3]

Shearography

Shearography, otherwise known as “out of plane gradient sensitive interferometer” is similar to ESPI, but measures the change in surface displacement gradient instead of the change in surface displacement. One of its primary uses is to detect surface and sub-surface flaws present in objects. It too can be used to investigate large areas quickly and easily, but presently is unable to accurately quantify the precise size, shape or extent of a flaw. A typical shearography layout is shown in Figure 2. The mirrors are arranged to shear the object image, and these two sheared images interfere with each other. Figure 2(b) shows how the same point on the object’s surface is viewed by the camera. A point A on the image is sheared through a distance S to point A’ by the mirrors. Because shearography measures the rate of displacement of a point relative to another, and not relative to an initial reference point as is the case with ESPI, it is much less sensitive to external vibration. [2]

As in the case of ESPI, an image of the object under investigation is captured using a computer in its unstressed state, the object stressed, and an image is taken in its stressed state. The two images are compared with each other by the computer and a fringe pattern is generated. The fringes represent lines of constant surface displacement gradient.

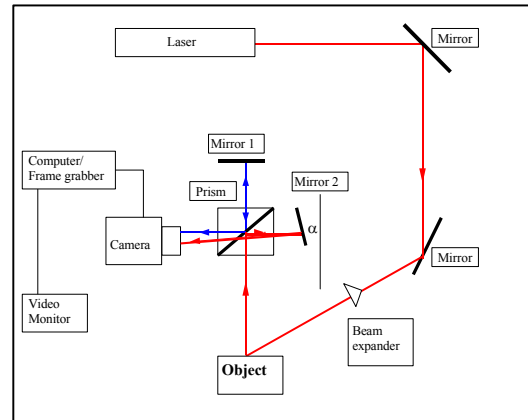


Figure 2 Shearography layout

The deflection gradient of the object surface at a point relative to another can be calculated by counting the number of fringes between the two points and applying equation 3.

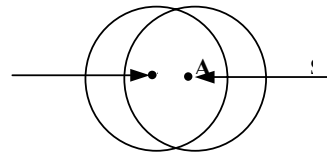


Figure 2(b) Shearing of image

$$\frac{\partial d}{\partial x_2} = \frac{N\lambda}{2S} \quad \text{Eqn 3}$$

Where $\frac{\partial d}{\partial x_2}$ is the displacement gradient, N is the total number of fringes, λ is the wavelength of the laser and S is the separation distance of any point in the sheared image. The sensitivity of this technique can be adjusted by altering the angle α , which increases the shift S between the images. [2]

Mechanical Impedance Analysis

Mechanical Impedance Analysis is a NDT technique that can be used to detect sub-surface flaws. It works on the premise that any structure subjected to forced vibration will oscillate locally with a certain amplitude and phase angle, relative to the applied vibration, which is dependent on certain physical material properties such as stiffness and damping, as illustrated in Figure 3(a). Flawed regions will clearly have different properties when compared to other regions and hence so will have different amplitude and phase responses. MIA compares the object response to previously defined “good” and “bad” regions.

The MIA equipment consists of a signal generator, a processor and associated electronics, and a probe containing two piezo-electric crystals as shown in Figure 3(b). One of the crystals is driven with a continuous sinusoidal signal by the signal generator. This vibration is transferred onto the test piece via the probe and the second crystal measures the response of the test piece to this vibration and returns it to the

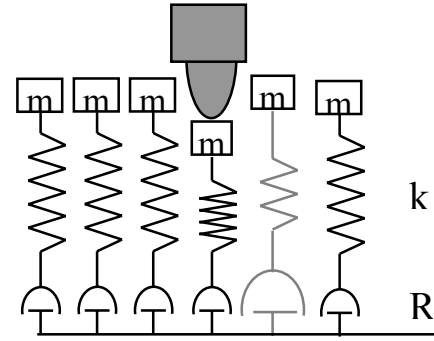


Figure 3(a) Schematic of object

processor for analysis. The resultant phase and amplitude response is shown in real time on a cathode ray tube display in a bar-graph format, and limits for the acceptability of flaws can be set. [4]

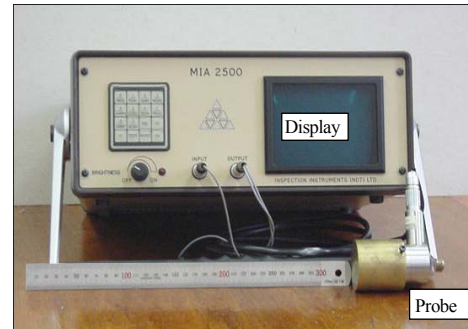


Figure 3(b) MIA Equipment

The impedance of the object's surface is given by Equation 4

$$Z = R_s + j(\omega m - k/\omega) \quad \text{Eqn 4}$$

The amplitude response of the surface can be calculated using Equation 5

$$y = \frac{F_0 e^{j(\omega t - \pi/2 - \theta)}}{\omega |Z_s|} \quad \text{Eqn 5}$$

The phase response of the object can be calculated using Equation 6

$$\theta = \tan^{-1} \left(\frac{X_s}{R_s} \right) \quad \text{Eqn 6}$$

where m is the local mass

k is the local stiffness

R is the local damping

ω is the angular velocity of the forced vibration

Experimental Procedure

ESPI Testing

The aircraft fin tested was a fibreglass/epoxy composite, and was in an as-manufactured state. ESPI was used to investigate several possible manufacturing flaws (marked A). These included air inclusions in the structure and areas where the epoxy had not bonded well to the fibreglass. Other flaws were also investigated such as a delamination (marked B, approx. 20x20mm) and an impact damage area

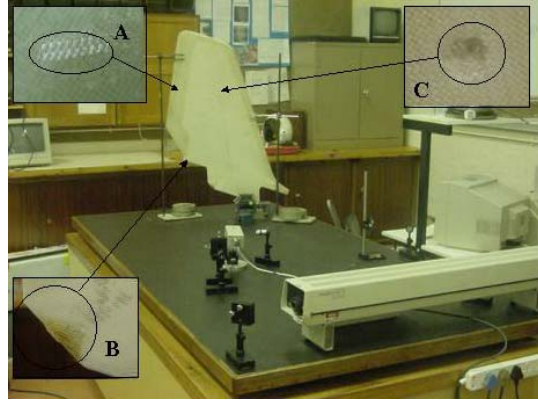


Figure 4 ESPI Testing of fin

(marked C, approx. 6mm diameter). A hair dryer and spotlight were used to create thermal stresses in the object for the investigation. By varying where the heat was applied, various different effects were noticed. When heating the area under investigation directly, fringes were created as a result of thermal expansion of the surface. Because of a disruption in heat flow around a flaw, differential isotherms were created in this region, and hence differential expansion. By heating indirectly from the opposite side of the fin, thermal expansion gave rise to mechanical stresses around the flaw.

A helicopter tail rotor section was also tested using the same procedure. It had two artificial flaws created on its surface, namely a pinhole (approx. 1mm diameter) and a slit (approx. 20 x 0.5mm). The slit was designed to simulate a crack in the blade surface

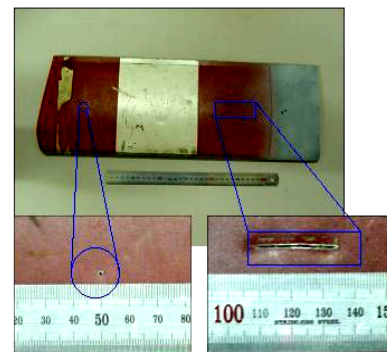


Figure 5 Tail rotor with flaws

Shearography and MIA Testing

The South African Airforce operates a number of Alouette III helicopters, and the construction of the main blade is shown in Figure 6. An alloy skin is shaped around and bonded to the spar, which determines the leading edge shape. It is then riveted to the along the trailing edge, and the cavity is filled with moltoprene foam. The spar is the main structure of the blade running along its length that supports the loads generated by drag and lift forces. The moltoprene helps maintain the shape of the trailing edge.

These blades currently two-tier NDT program. The first level is a visual inspection for cracks in cuff near the point of attachment and is performed every 25 hours of use. If cracks are suspected in this region, the blades are removed and further tested using dye-penetrant. The second level of investigation occurs after every 100 hours of use or every six months, where the blades are checked for cracks and delaminations between the spar and outer skin. Presently, delaminations are

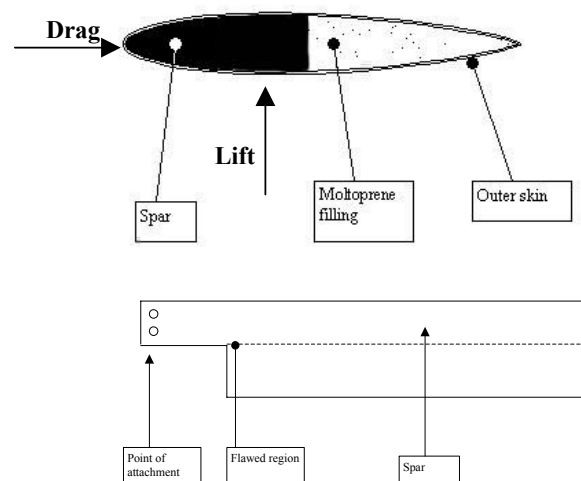


Figure 6 Alouette III main blade construction

located by tapping the blades over the entire area with a purpose-made tapping hammer and listening for variations in the response. If any delaminations are located and are above a certain size, the blades are sent to the manufacturer for further inspection and possible repair or replacement, which can be costly. If the blade is returned to service without being repaired or replaced, the blade must be removed and the debonded region re-inspected every 25 hours subsequently to monitor its growth rate. [8]

An alternative to the tapping technique was investigated because:

- The results are not repeatable.
- Each person will have his or her own idea of what is acceptable or not, as well as having a different hearing sensitivity. As a result, results can be expected to vary widely from person to person.

- There is no permanent record of the results, which may be used to study the rate at which the flaw grows accurately.
- Only large and obvious flaws are readily detected[6]
- This technique is very time-consuming, typically taking three hours to complete.[8]

Shearography was investigated as such an alternative. It was hoped that shearography would be able to locate these delaminations quickly and if successful, replace the current technique. The blades were supported and secured. An image of the specimen blade was captured in its normal, unstressed state using the shearography equipment. Thermal stresses were then generated in the specimens by illuminating them with a powerful spotlight for a few seconds over the area being investigated. An image of the blade in this stressed state was captured. The computer software processed the results and the fringe pattern was generated and stored. The presumption was that a delamination between the spar and outer skin would affect localised heat flow, and would manifest itself in the fringe pattern obtained.

MIA was then performed on the whole area to locate and quantify the size, shape and precise location of any flaws and to verify the shearography results. Limits of power, gain and what constituted a good and bad area were set for blade's surface. A sheet of paper laid on blade surface and the probe traced across surface. Areas that were indicated as bad were mapped on the sheet of paper. Rivets on the blade's inner edge were marked on the paper and used as reference points. Comparison was then made between the shearography and MIA results.

Figure 7 shows a typical MIA scan, indicating the location of the spar and the leading and trailing edges and flawed regions.

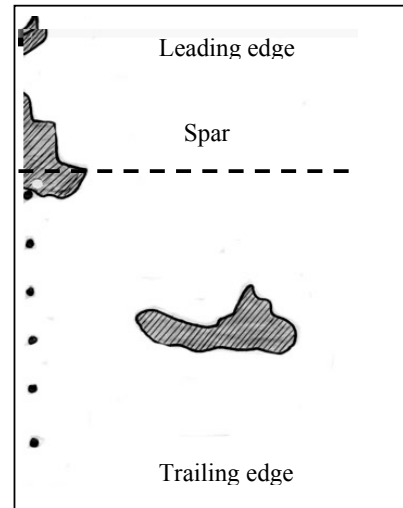


Figure 7 MIA scan of blade

Results

ESPI results

The ESPI did not indicate any structural defects when testing flaws present from manufacturing that were visible on the object surface. The induced flaws were however easily located. Figure 8(a) shows the ESPI image of direct heating on the impact damage area, highlighted by the irregular fringe line. Figure 8(b) shows the ESPI image of the impact damage area stressed by heating the fin away from the flaw and figure 8(c) heating on the opposite side of the fin. Figure 8(d) shows the ESPI image of the delaminated region stressed by local heating and figure 8(e) mechanical stresses. Figure 8(f) shows the slit flaw in the tail rotor stressed by localised heating. Figure 8(g) shows the ESPI image of an internal flaw located by ESPI. This was not visible on the rotor's surface, and was located during ESPI inspection of the blade. Figure 8(h) shows the ESPI image of the pinhole flaw that can be seen as a result of the irregular fringe pattern.

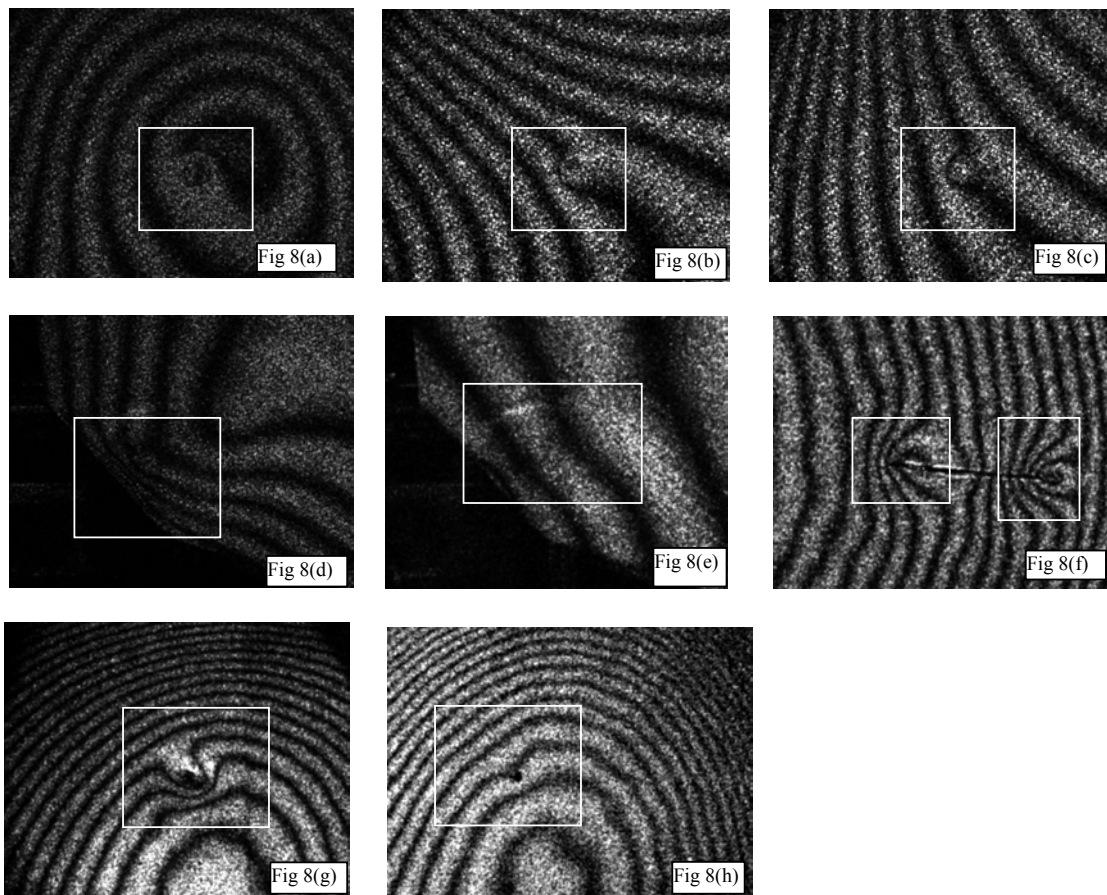


Figure 8 ESPI results

Shearography and MIA results

The images in Figure 9,10 and 11 show the shearography and MIA images for three of the blades that were tested. The leading edge is towards the top of the page and the spar is visible on the left as it emerges from the blade. The black spots on the MIA images were rivets on the blade that were marked to provide reference points.

The shearography pattern in Figure 9 shows fringes in the spar area that are closely arranged and irregular, and is a possible indication of a flaw being present. The MIA and shearography scans appear to correlate for this flaw. There were two flaws in the middle and lower right of the MIA scan that were not detected by shearography. These would most likely have been debonding

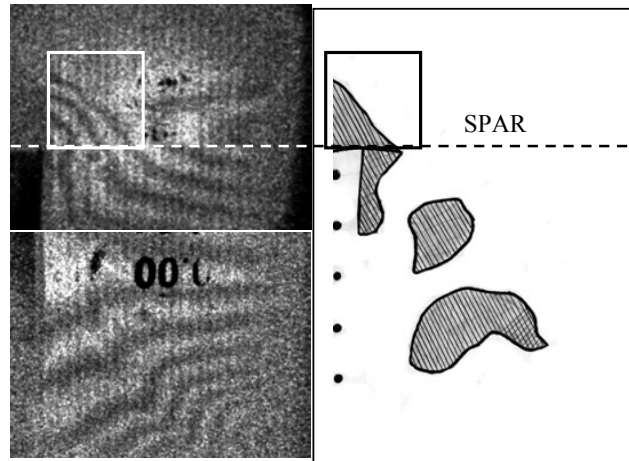


Figure 9 Shearography and MIA results for blade 14546

between the outer skin and internal moltoprene filling.

In the lower shearography image of the trailing edge, the irregular fringe pattern marks the location of an alloy reinforcing rib on the blade. It shows up because of differential heat flow in this region compared to other areas of the blade.

In a subsequent test, both the MIA and shearography indicated a flaw near the spar. This is shown by the irregular fringe pattern in Figure 10 in the upper left area of the shearography image. Flaws indicated by MIA behind the spar were not indicated by shearography, although this is not critical, as these flaws are between the moltoprene foam and outer skin, which is not a structural part of the blade.

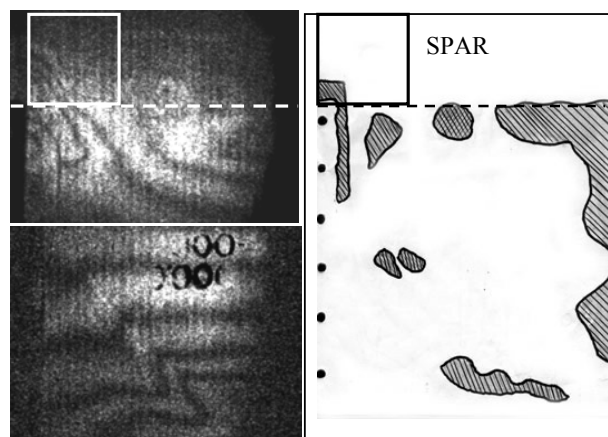


Figure 10 Shearography and MIA for blade 7093

MIA on this blade did not indicate a flaw near the spar. There were no fringes in the spar region of this blade. This was because the heat in this region had already been dissipated into the spar itself through the good bond between the outer skin and the steel spar. If there was a delamination between the spar and outer skin, a void would exist between them, and the heat

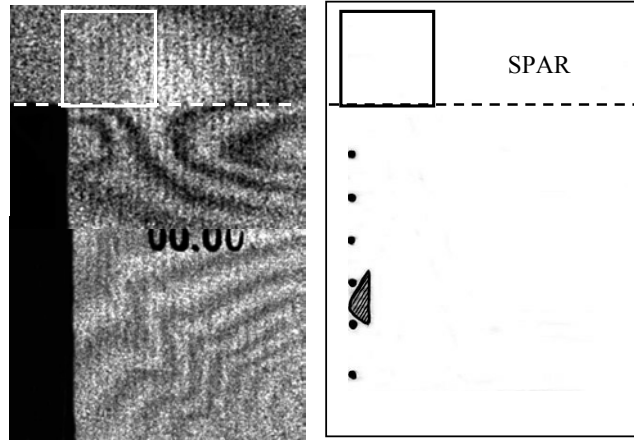


Figure 11 Shearography and MIA for blade 14460

would not be able to dissipate as quickly, and fringes would be observed in this area. The peculiar pattern below the highlighted area is localised around a rivet. A possible flaw is indicated, which maybe a debond or loose rivet at this point. Again the kinked fringe in the trailing edge region is as a result of the reinforcing rib.

Conclusions

ESPI was able to locate both the impact damage and delamination flaws in the fibreglass/epoxy composite fin. It was, however, unable to locate the manufacturing defects. An alternative stressing technique may highlight this type of flaw more effectively. ESPI was able to locate the slit in the tail rotor blade, as well as the pinhole flaw. ESPI was able to locate an internal flaw in the rotor blade that was not visible to the naked eye, which may have otherwise gone unnoticed. Although the fringes only give a qualitative indication of the flaw, the inspection takes less than a minute to perform once it has been set up. Additionally, large areas can be inspected at once, making this method a practical alternative to many current methods.

Generally the shearography and MIA techniques agreed with each other for flaws on the spar, but not on the trailing edge. Shearography is suitable for locating flaws over a large surface area, but is unable to quantify it in terms of size and severity. It is able to accurately predict the presence or absence of a flaw in this region. As a result, MIA only needs to be performed if shearography indicates a flaw at the spar, and is not necessary if it does not. The MIA

technique is well suited to quantifying a flaw, once it has been located. It is therefore worth investigating further. A standard approach to the use of the MIA equipment specifically for use on the blades should be developed, and limits of acceptable and unacceptable flaws obtained.

The direct quantification of flaws with ESPI and shearography may be possible if a standard test procedure for stress application and a database of expected results is developed. This would make these techniques very difficult to rival with a lot of other methods that are presently employed.

References

1. J. Gryzagoridis, D. Findeis, D.F. van Zyl, J.R. Myles 'ESPI – a viable NDE tool for plant extension' *International Journal of Pressure Vessels and Piping*, 73 (1997) 25 - 32
2. J. Gryzagoridis *Holographic and Electronic Speckle Pattern Interferometry and Shearography*
3. Various *Non Destructive Testing ASM Handbook Series No.17*
4. MIA manual
5. J. Gryzagoridis, D. Findeis, D.R. Schneider 'The Impact of Optical Methods In Vessel Fracture Protection' *International Journal of Pressure Vessels and Piping*, 61 (1995) 457 – 469
6. P.R. Teagle *Recent Advances in Mechanical Impedance Analysis Instrumentation For The Evaluation of Adhesive Bonded and Composite Structures* 1985
7. Jones R., Wykes C., *Holographic and Speckle Interferometry*, 1st Ed. Cambridge University Press 1983
8. D. Findeis, J Gryzagoridis *The Feasibility of Optical Interference-based NDE Methods to Inspect Helicopter Rotor Blades* SPIE Vol. 3994 (2000) pp 59 – 67